

# Towards high sensitivity gas detection with hollow-core photonic bandgap fibers

Fan Yang,<sup>1,2</sup> Wei Jin,<sup>1,2,\*</sup> Yingchun Cao,<sup>1</sup> Hoi Lut Ho,<sup>2</sup> and Yiping Wang<sup>3</sup>

<sup>1</sup>The Hong Kong Polytechnic University Shenzhen Research Institute, Shenzhen, China

<sup>2</sup>Department of Electrical Engineering, The Hong Kong Polytechnic University, Hong Kong, China

<sup>3</sup>College of Optoelectronic Engineering, Shenzhen University, Shenzhen, China

\*eewjin@polyu.edu.hk

**Abstract:** This paper investigates the effect of modal interference on the performance of hollow-core photonic bandgap fiber (HC-PBF) gas sensors. By optimizing mode launch, using proper length of sensing HC-PBF, and applying proper wavelength modulation in combination with lock-in detection, as well as appropriate digital signal processing, an estimated lower detection limit of less than 1 part-per-million by volume (ppmv) acetylene is achieved.

©2014 Optical Society of America

**OCIS codes:** (060.2370) Fiber optics sensors; (060.5295) Photonic crystal fibers; (060.4005) Microstructured fibers; (060.4080) Modulation; (280.4788) Optical sensing and sensors.

## References and links

1. R. F. Cregan, B. J. Mangan, J. C. Knight, T. A. Birks, P. St. J. Russell, P. J. Roberts, and D. C. Allan, "Single-mode photonic band gap guidance of light in air," *Science* **285**(5433), 1537–1539 (1999).
2. Y. L. Hoo, W. Jin, H. L. Ho, J. Ju, and D. N. Wang, "Gas diffusion measurement using hollow-core photonic bandgap fiber," *Sens. Actuators B Chem.* **105**(2), 183–186 (2005).
3. T. Ritari, J. Tuominen, H. Ludvigsen, J. C. Petersen, T. Sørensen, T. P. Hansen, and H. R. Simonsen, "Gas sensing using air-guiding photonic bandgap fibers," *Opt. Express* **12**(17), 4080–4087 (2004).
4. A. Brakel, C. J. Misas, T. T. Ng, P. Petropoulos, J. P. Dakin, C. Grivas, M. N. Petrovich, and D. J. Richardson, "Cavity ring-down in a photonic bandgap fiber gas cell," in *Conference on Lasers and Electro-Optics*, (Optical Society of America, 2008), paper CThEE4.
5. H. Lehmann, H. Bartelt, R. Willsch, R. Amézeua-Correa, and J. C. Knight, "In-line gas sensor based on a photonic bandgap fiber with laser-drilled lateral microchannels," *IEEE Sens. J.* **11**(11), 2926–2931 (2011).
6. X. Li, J. Liang, S. Lin, Y. Zimin, Y. Zhang, and T. Ueda, "NIR spectrum analysis of natural gas based on hollow-core photonic bandgap fiber," *IEEE Sens. J.* **12**(7), 2362–2367 (2012).
7. A. M. Cubillas, M. Silva-Lopez, J. M. Lazaro, O. M. Conde, M. N. Petrovich, and J. M. Lopez-Higuera, "Methane detection at 1670-nm band using a hollow-core photonic bandgap fiber and a multiline algorithm," *Opt. Express* **15**(26), 17570–17576 (2007).
8. F. Magalhães, J. P. Carvalho, L. A. Ferreira, F. M. Araújo, and J. L. Santos, "Methane detection system based on wavelength modulation spectroscopy and hollow-core fibres," in *Proceedings of IEEE Sensors Conference* (IEEE, 2008), pp. 1277–1280.
9. R. M. Wynne, B. Barabadi, K. J. Creedon, and A. Ortega, "Sub-minute response time of a hollow-core photonic bandgap fiber gas sensor," *J. Lightwave Technol.* **27**(11), 1590–1596 (2009).
10. K. S. Lee, Y. K. Lee, and S. H. Jang, "A novel grating modulation technique for photonic bandgap fiber gas sensors," *IEEE Photon. Technol. Lett.* **23**(10), 624–626 (2011).
11. J. P. Parry, B. C. Griffiths, N. Gayraud, E. D. McNaghten, A. M. Parkes, W. N. MacPherson, and D. P. Hand, "Towards practical gas sensing with micro-structured fibres," *Meas. Sci. Technol.* **20**(7), 075301 (2009).
12. M. N. Petrovich, F. Poletti, and D. J. Richardson, "Analysis of modal interference in photonic bandgap fibres," in *International Conference on Transparent Optical Networks* (ICTON, 2010), pp. 1–4.
13. W. Jin, H. L. Ho, Y. C. Cao, J. Ju, and L. F. Qi, "Gas detection with micro- and nano-engineered optical fibers," *Opt. Fiber Technol.* **19**(6), 741–759 (2013).
14. M. N. Petrovich, F. Poletti, A. Van Brakel, and D. J. Richardson, "Robustly single mode hollow core photonic bandgap fiber," *Opt. Express* **16**(6), 4337–4346 (2008).
15. J. K. Lyngso, C. Jakobsen, H. R. Simonsen, and J. Broeng, "Single-mode 7-cell core hollow core photonic crystal fiber with increased bandwidth," *Proc. SPIE* **7753**, 77533Q (2011).
16. J. M. Fini, J. W. Nicholson, R. S. Windeler, E. M. Monberg, L. Meng, B. Mangan, A. Desantolo, and F. V. DiMarcello, "Low-loss hollow-core fibers with improved single-modedness," *Opt. Express* **21**(5), 6233–6242 (2013).
17. J. W. Nicholson, L. Meng, J. M. Fini, R. S. Windeler, A. De Santolo, E. Monberg, F. DiMarcello, Y. Dulashko, M. Hassan, and R. Ortiz, "Measuring higher-order modes in a low-loss, hollow-core, photonic-bandgap fiber," *Opt. Express* **20**(18), 20494–20505 (2012).

18. K. Z. Aghaie, M. J. F. Digonnet, and S. Fan, "Experimental assessment of the accuracy of an advanced photonic-bandgap-fiber model," *J. Lightwave Technol.* **31**(7), 1015–1022 (2013).
19. M. Li, J. A. West, and K. W. Koch, "Modeling effects of structural distortions on air-core photonic bandgap fibers," *J. Lightwave Technol.* **25**(9), 2463–2468 (2007).
20. A. Yariv and P. Yeh, *Photonics: Optical Electronics in Modern Communications* (Oxford University Press, 2007), Chap. 2.
21. A. W. Snyder and J. D. Love, *Optical Waveguide Theory* (Chapman & Hall, 1983), Chap. 20.
22. G. Stewart, A. Mencaglia, W. Philp, and W. Jin, "Interferometric signals in fiber optic methane sensors with wavelength modulation of the DFB laser source," *J. Lightwave Technol.* **16**(1), 43–53 (1998).
23. D. T. Cassidy and J. Reid, "Harmonic detection with tunable diode lasers—two-tone modulation," *Appl. Phys. B* **29**(4), 279–285 (1982).
24. C. B. Carlisle, D. E. Cooper, and H. Preier, "Quantum noise-limited FM spectroscopy with a lead-salt diode laser," *Appl. Opt.* **28**(13), 2567–2576 (1989).
25. H. C. Sun and E. A. Whittaker, "Novel étalon fringe rejection technique for laser absorption spectroscopy," *Appl. Opt.* **31**(24), 4998–5002 (1992).
26. H. Riris, C. B. Carlisle, R. E. Warren, and D. E. Cooper, "Signal-to-noise ratio enhancement in frequency-modulation spectrometers by digital signal processing," *Opt. Lett.* **19**(2), 144–146 (1994).
27. H. Riris, C. B. Carlisle, L. W. Carr, D. E. Cooper, R. U. Martinelli, and R. J. Menna, "Design of an open path near-infrared diode laser sensor: application to oxygen, water, and carbon dioxide vapor detection," *Appl. Opt.* **33**(30), 7059–7066 (1994).
28. L. Xiao, M. S. Demokan, W. Jin, Y. Wang, and C.-L. Zhao, "Fusion splicing photonic crystal fibers and conventional single-mode fibers: microhole collapse effect," *J. Lightwave Technol.* **25**(11), 3563–3574 (2007).
29. Y. L. Hoo, W. Jin, C. Shi, H. L. Ho, D. N. Wang, and S. C. Ruan, "Design and modeling of a photonic crystal fiber gas sensor," *Appl. Opt.* **42**(18), 3509–3515 (2003).
30. Y. Cao, "Quartz-enhanced photoacoustic spectroscopy and its association with fiber-optic devices," Ph.D. Thesis, The Hong Kong Polytechnic University (2012).
31. G. B. Rieker, J. B. Jeffries, and R. K. Hanson, "Calibration-free wavelength-modulation spectroscopy for measurements of gas temperature and concentration in harsh environments," *Appl. Opt.* **48**(29), 5546–5560 (2009).
32. G. Stewart, W. Johnstone, J. R. P. Bain, K. Puxton, and K. Duffin, "Recovery of absolute gas absorption line shapes using tunable diode laser spectroscopy with wavelength modulation-part 1: Theoretical analysis," *J. Lightwave Technol.* **29**(6), 811–821 (2011).

## 1. Introduction

A hollow-core photonic bandgap fiber (HC-PBF) allows the confinement of an optical mode and gas- or liquid-phase materials simultaneously within the hollow-core and provides an ideal platform for strong light-matter interaction over a long distance. The possibility of using HC-PBFs for gas detection was suggested by Cregan et al. as early as the first air/silica HC-PBFs were demonstrated in 1999 [1]. In 2004, Hoo et al. reported online the results of gas diffusion measurement with a HC-PBF [2]. A short while later, Ritari et al. reported high sensitivity gas detection using HC-PBFs with transmission windows centered at 1300 and 1500 nm [3]. Since then, several research groups have reported gas detection with HC-PBFs [4–10]. These works include the detection of different gas species such as  $C_2H_2$ ,  $C_2H_6$ ,  $CH_4$  and  $NH_3$ ; the application of different signal processing techniques such as cavity ring down spectroscopy [4], fiber Bragg grating modulation [10], multi-line fitting [7], and multi-component gas detection [5, 9].

However, the performance of gas detection was found limited by the modal interference (MI) in HC-PBFs [11–13]. Current commercial HC-PBFs support several groups of modes and the interference of these modes results in fluctuation of the transmitted light intensity, which sets a limit to the minimum detectable gas concentration. Efforts are being made to develop truly single-mode HC-PBFs with which the MI could be avoided. Petrovich et al. reported a single-mode HC-PBF with its core formed by removing three unit cells (i.e., 3-cell core) [14]. The diameter of the 3-cell core is ~35% smaller than the 7-cell core, and the transmission loss is significantly higher than the 7-cell core HC-PBFs. Lyngsø et al. reported a 7-cell core HC-PBF using a core tube with 80% wall-thickness relative to that of the cladding capillary tubes [15]. The single-mode region is near to the short wavelength bandgap edge and has a width of only 30 nm, which may not cover the absorption bands of some important gases. Recently, Fini et al. reported a low-loss 19-cell core HC-PBF by employing perturbed resonance to improve its single modedness [16]. However, so far there is no true single-mode HC-PBFs available on market.

In this paper, we study the characteristics of MI in the commercial HC-1550-02 fiber and study the effect of the MI on the performance of gas sensors based on such a fiber. By using proper the length of sensing fiber, optimizing the mode launch, employing wavelength modulation spectroscopy (WMS) with proper modulation parameters and digital signal processing, we demonstrate acetylene detection with a noise-equivalent detection limit of <1 ppmv (parts-per-million by volume).

## 2. Modes and modal interference in HC-PBF

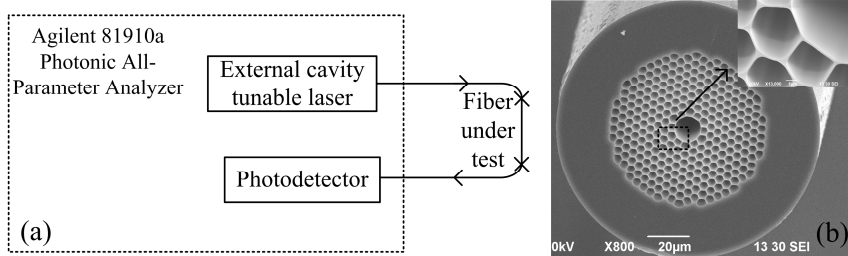


Fig. 1. (a) Setup for transmission spectrum measurement, (b) the scanning electron microscopy (SEM) image of HC-1550-02 fiber's cross-section.

Figure 1(a) shows the experimental setup. The wavelength-tunable external cavity diode laser and photo-detector within the Agilent 81910A Photonic All-Parameter Analyzer were used to measure the transmission spectrums of HC-PBF samples. The wavelength tuning range was set from 1525 to 1535 nm, with a tuning resolution of 0.001 nm. The fiber samples tested were prepared by fusion splicing different lengths of HC-1550-02 fiber (NKT Photonics) to standard single mode fibers (SMFs) at both ends. The scanning electron microscope (SEM) image of the HC-1550-02 fiber is shown in Fig. 1(b).

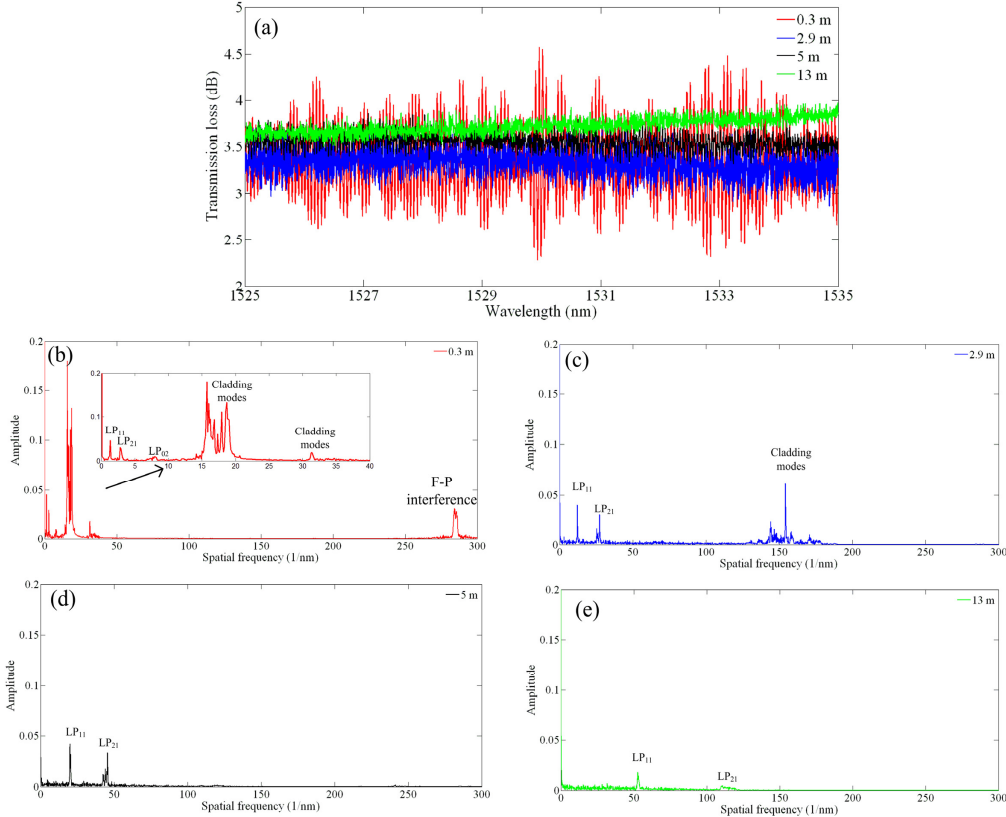


Fig. 2. (a) Transmission spectrums of HC-PBF samples with different lengths, and (b-e) Fourier transforms of the spectrums in (a).

Figure 2(a) shows the measured transmission spectrums of four samples with HC-PBF length ranging from 0.3 to 13 m. The spectrums are normalized by the spectrum measured directly from the source SMF pigtail. The magnitude of the interference signals reduced significantly for the 13 m HC-PBF sample while the average loss only increased slightly, as compared with the 0.3 m sample. The Fourier transforms of the interference spectrums are shown in Figs. 2(b)-2(e). Fourier transform has been used for analyzing interference between coherent modes with different group delays to study the modal properties of HC-PBFs [12, 17]. There are five groups of higher order modes that interfere with the fundamental mode and these modes are labeled for the 0.3 m long HC-PBF sample as shown in the inset of Fig. 2(b). As will be discussed later in this section, the first three peaks in the inset correspond to three higher order groups of core modes. The peaks with higher spatial frequencies correspond to higher differential group refractive indexes (0.08-0.2) and may be due to MI from cladding modes [12].

We investigated the characteristics of the cladding modes by examining the output mode intensity patterns of HC-1550-02 fiber samples with different lengths and launching offset relative to the input SMF. Figure 3 shows the near-field mode profiles at 1530 nm recorded by use of a charge-coupled device (CCD) camera. The mode intensity pattern of a 35 m long sample showed no obvious change with the launch offset other than power variations, as shown in Figs. 3(a)-3(c). For the 110 cm long sample, the mode intensity pattern changed significantly with launch offset, as shown in Figs. 3(d)-3(f). With 6  $\mu\text{m}$  offset excitation, a significant fraction of power resides outside the core. The cladding modes exist after 110-cm transmission but would be significantly attenuated after propagating through the 35-m-long sample.

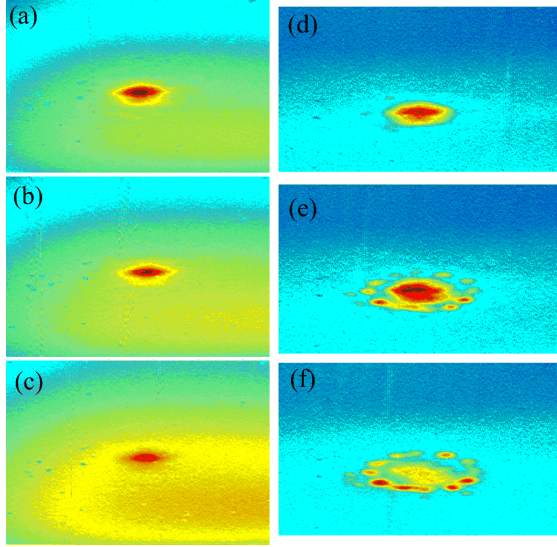


Fig. 3. Output mode intensity profile of 35 m HC-1550-02 fiber with (a) optimal launch, (b) 3  $\mu\text{m}$  offset launch, (c) 6  $\mu\text{m}$  offset launch. Output mode intensity profile of 110 cm HC-1550-02 fiber with (d) optimal launch, (e) 3  $\mu\text{m}$  offset launch, (f) 6  $\mu\text{m}$  offset launch.

Fabry-Perot type interference due to reflected waves from the SMF/HC-PBF interfaces is also observable in Fig. 2(b). The spatial frequencies of the interference signals increase with the length of the HC-PBF samples while the magnitudes decrease. The rate of decrease in magnitude is much faster for the cladding modes than for the core modes, and this is expected because the attenuations of the cladding modes are much larger. For the 0.3 m sample, the interference between the core and the cladding modes are dominant, as can be seen from Fig. 2(b). The interferences between the cladding modes and the fundamental core mode becomes minimal for fiber samples longer than 5 m as shown in Figs. 2(d) and 2(e), although the mode beatings between the core modes still exist. For the 13-m long sample, the interference between the core modes is also significantly reduced as shown in Fig. 2(e).

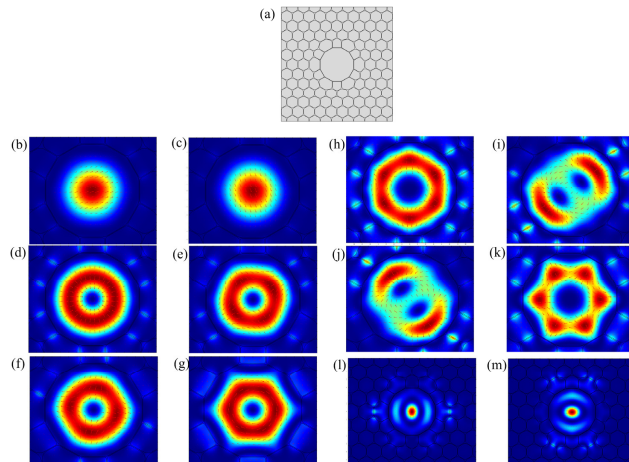


Fig. 4. (a) Geometry model of HC-1550-02 fiber used for calculating mode contents, (b) and (c) are the mode fields of HE<sub>11</sub> modes, (d)-(g) are the mode fields of quasi-TM<sub>01</sub>, odd HE<sub>21</sub>, even HE<sub>21</sub> and quasi-TE<sub>01</sub> modes respectively, (h)-(k) are the mode fields of odd HE<sub>31</sub>, odd EH<sub>11</sub>, even EH<sub>11</sub>, and even HE<sub>31</sub> modes, (l) and (m) are the mode fields of odd HE<sub>12</sub> and even HE<sub>12</sub> modes.

The core modes of the HC-1550-02 fiber were investigated by use of COMSOL Multiphysics 4.2 software. The model structure used is the same as described by Aghaie [18] and shown in Fig. 4(a). The core diameter and pitch of the fiber are 11.64 and 3.88  $\mu\text{m}$  respectively. The calculated mode fields of the four groups of core modes are shown in Figs. 4(b)-4(m). The phase effective refractive index (RI) of different modes as functions of wavelength were calculated with COMSOL, and the group RI of the modes were then calculated by using

$$n_{\text{effg}}(\lambda) = n_{\text{effp}}(\lambda) - \lambda \cdot dn_{\text{effp}}(\lambda) / d\lambda \quad (1)$$

where  $n_{\text{effg}}$  and  $n_{\text{effp}}$  are the group RI and phase RI, respectively and  $\lambda$  is the wavelength. Table 1 lists the calculated phase and group RI, as well as the calculated and measured differential group RI for the LP<sub>11</sub>, LP<sub>21</sub> and LP<sub>02</sub> mode groups that beat with the LP<sub>01</sub> mode. The experimental differential group RI was derived by the half width half maximum of the first three peaks in Fig. 2(b) with 30 cm HC-1550-02 fiber sample. The discrepancy between the calculated and experimentally measured differential group RI may result from the difference between the real structure of HC-1550-02 fiber and the model structure we used to calculate the mode field since the properties of HC-PBFs are extremely sensitive to changes of the structural parameters [19].

**Table 1. Calculated phase, group and differential group RI, and measured differential group RI at 1530 nm**

Fiber modes		Phase RI	Group RI	Calculated differential group RI	Measured differential group RI
LP <sub>01</sub>	HE <sub>11</sub> <sup>(1,2)</sup>	0.994423	1.012018	~	~
LP <sub>11</sub>	quasi-TM <sub>01</sub>	0.987124	1.029964	0.017946	0.0101-0.0109
	HE <sub>21</sub> <sup>(1,2)</sup>	0.986717	1.026497	0.014479	
	quasi-TE <sub>01</sub>	0.986219	1.029059	0.017041	
LP <sub>21</sub>	HE <sub>31</sub> <sup>1</sup>	0.978444	1.049589	0.037571	0.0211-0.0240
	EH <sub>11</sub> <sup>(1,2)</sup>	0.978237	1.050147	0.038129	
	HE <sub>31</sub> <sup>2</sup>	0.977954	1.048334	0.036316	
LP <sub>02</sub>	HE <sub>12</sub> <sup>1</sup>	0.975318	1.060233	0.048215	0.0562-0.0652
	HE <sub>12</sub> <sup>2</sup>	0.975315	1.060995	0.048977	

### 3 Reduction of MI with optimal mode launch

We studied MI for a fiber sample shown in Fig. 5. The output end of a 13-m-long HC-1550-02 fiber is fusion spliced to a SMF while its input end is jointed to another SMF by use of a mechanical splicer. The gap between the SMF and HC-PCF ends at the joint can be varied and viewed by use of an optical microscope. Because of the different outer diameters of the SMF and HC-1550-02 fiber, lateral offset would result at the SMF/HC-PBF joint. The quoted inner diameter of the mechanical splice, the cladding diameters of the SMF and HC-1550-02 fiber are respectively 125.3, 125 and 120  $\pm$  1  $\mu\text{m}$ . Therefore, the lateral offset between the cores of the SMF and HC-1550-02 fiber would be in the range of 2-3  $\mu\text{m}$ .

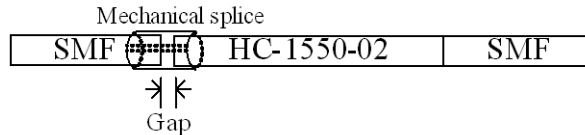


Fig. 5. A HC-PBF sample with its input end mechanical spliced to a SMF with a gap

The transmission characteristics of the fiber sample were measured with the same setup shown in Fig. 1. Figures 6(a) and 6(b) show the normalized transmission spectrums and the corresponding Fourier transforms of the 13 m long HC-1550-02 fiber sample with different gaps. MI due to two groups of modes (i.e., LP<sub>11</sub> and LP<sub>21</sub> groups) is observable in Fig. 6. The magnitudes of the interference signals decrease considerably when the gap is varied from 0 to

100  $\mu\text{m}$ . Further increase in gap-size results in a little reduction in the interference signal but with significant increase in the joint loss. Hence, a 100  $\mu\text{m}$  gap may be regarded as optimal for reducing MI and at the same time maintaining a reasonably low joint-loss.

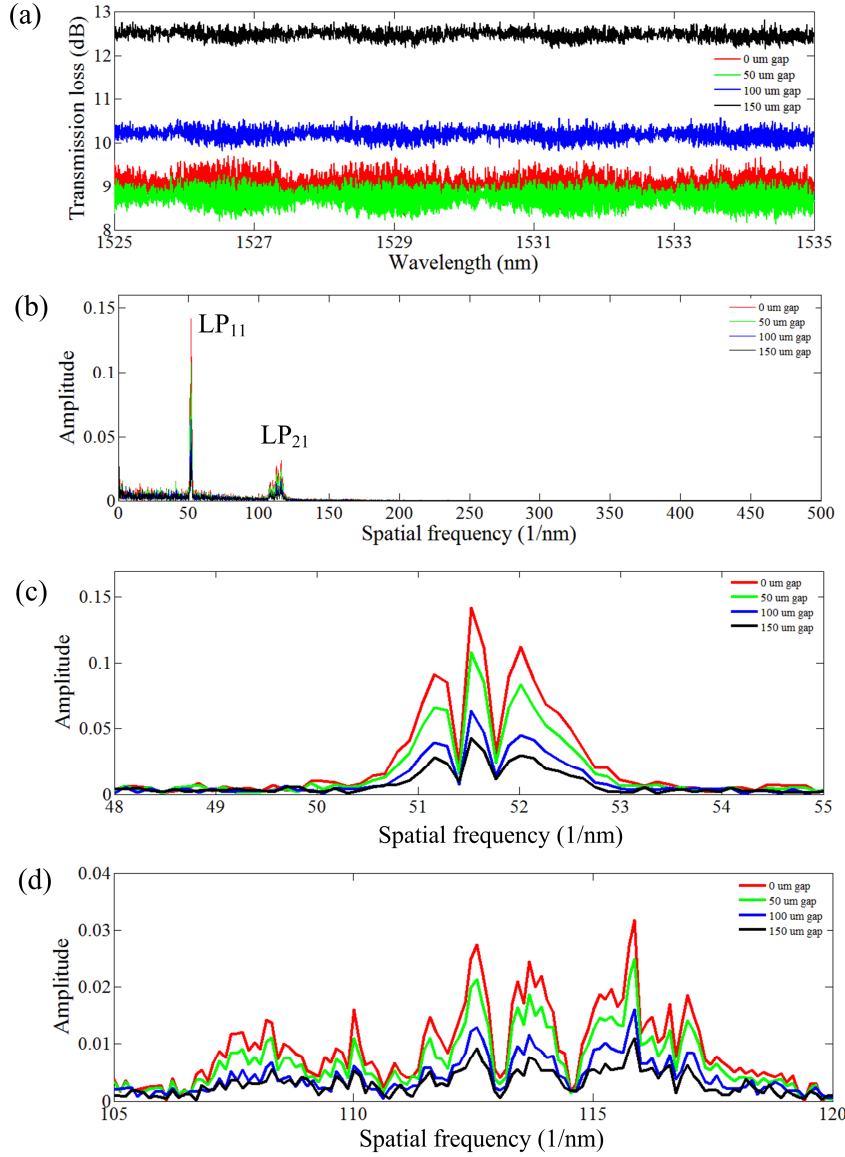


Fig. 6. (a) Normalized transmission spectrums of 13 m HC-1550-02 fiber with different gap sizes, and (b) Fourier transforms of the transmission spectrums in (a). Details of the mode beatings in (b) are shown in (c) for LP<sub>11</sub> and in (d) for LP<sub>21</sub>.

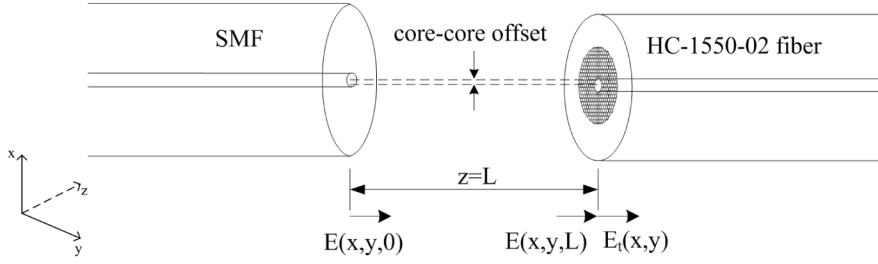


Fig. 7. Mode excitation from SMF to HC-1550-02 fiber.

We also carried out theoretical analysis and numerical simulation on the effect of gap and lateral offset on the mode launch or excitation efficiencies by use of a model structure shown in Fig. 7. Light from the SMF gets diffracted in the air before coupling into the HC-1550-02 fiber. Supposing the polarization direction of the electric field is in the x direction shown in Fig. 7, the mode field of the SMF may be approximated to be a Gaussian profile and the electric field at the output end of the SMF, i.e.,  $z = 0$ , may be written as

$$E(x, y, 0) = E_0 \exp\left[-(x^2 + y^2)/a^2\right] \quad (2)$$

where  $a$  is the mode field radius,  $E_0$  the field amplitude at the center of the beam.

The electric field amplitude in air at  $z = L$  can then be written as [20]

$$E(x, y, L) = \frac{E_0 e^{-ikL}}{1 - i \frac{\lambda L}{\pi a^2}} \exp\left(-i \frac{k}{2R}(x^2 + y^2)\right) \exp\left(-\frac{x^2 + y^2}{\omega^2}\right) \quad (3)$$

with  $R = L + \frac{1}{L} \left(\frac{\pi a^2}{\lambda}\right)^2$ ,  $\omega^2 = a^2 \left(1 + \left(\frac{L\lambda}{\pi a^2}\right)^2\right)$ , where  $k$  is the wave number,  $L$  the gap between HC-PBF and SMF. A similar expression exists for the magnetic field  $H(x, y, L)$ .

At the input end (i.e.,  $z = L$ ) of the HC-1550-02 fiber, the transverse electric and magnetic field may be expressed as

$$E_t(x, y) \equiv \frac{2n_{air}}{n_{air} + n_{HC}} E(x, y, L) \quad (4)$$

$$H_t(x, y) \equiv \frac{2n_{HC}}{n_{air} + n_{HC}} H(x, y, L) \quad (5)$$

Because  $n_{HC} \approx n_{air}$ , Eqs. (4) and (5) may be re-written as [21]

$$E_t(x, y) \equiv E(x, y, L) \quad (6)$$

$$H_t(x, y) \equiv H(x, y, L) \quad (7)$$

Within the HC-1550-02 fiber, a range of bound and leaky modes are excited and they are related to  $E_t(x, y)$  and  $H_t(x, y)$  by:

$$E_t(x, y) = \sum_j a_j e_j(x, y) + E_{tr}(x, y) \quad (8)$$

$$H_t(x, y) = \sum_j a_j h_j(x, y) + H_{tr}(x, y) , \quad (9)$$

where  $a_j$  is the amplitude of each bound modes.  $e_{ij}$  and  $h_y$  are the transverse electric and magnetic fields of the bound modes.  $E_{tr}(x, y)$  and  $H_{tr}(x, y)$  represents the transverse electric and magnetic fields of leaky modes. All the bound modes are orthogonal to each other and to leaky modes, and the mode excitation amplitude may be evaluated by using

$$a_j = \frac{\int_{A_\infty} E_t \times h_y^* \cdot \hat{z} dA}{\int_{A_\infty} e_{ij} \times h_y^* \cdot \hat{z} dA} = \frac{\int_{A_\infty} e_{ij}^* \times H_t \cdot \hat{z} dA}{\int_{A_\infty} e_{ij}^* \times h_y \cdot \hat{z} dA} \quad (10)$$

With the above formulation, we calculated the mode launch amplitude for 2 and 3  $\mu\text{m}$  lateral offset for different longitudinal gaps and the results are shown in Fig. 8. The launch amplitude of the LP<sub>01</sub> (HE<sub>11</sub>) mode decreases approximately linearly with increasing gap size, while the launch amplitudes of the higher order core modes such as LP<sub>11</sub> (TE<sub>01</sub>, odd HE<sub>21</sub>, even HE<sub>21</sub>) and LP<sub>21</sub> (even HE<sub>31</sub>) modes decrease more significantly for gap from 0 to 100  $\mu\text{m}$  but very little from 100 to 150  $\mu\text{m}$ . The launch amplitudes of TM<sub>01</sub>, odd HE<sub>31</sub>, odd EH<sub>11</sub> and even EH<sub>11</sub> modes are 5-6 orders lower than the fundamental mode and we did not plot them in Fig. 8. Hence a gap-size of 100  $\mu\text{m}$  may be an optimal value, which agrees with the experimental observation.

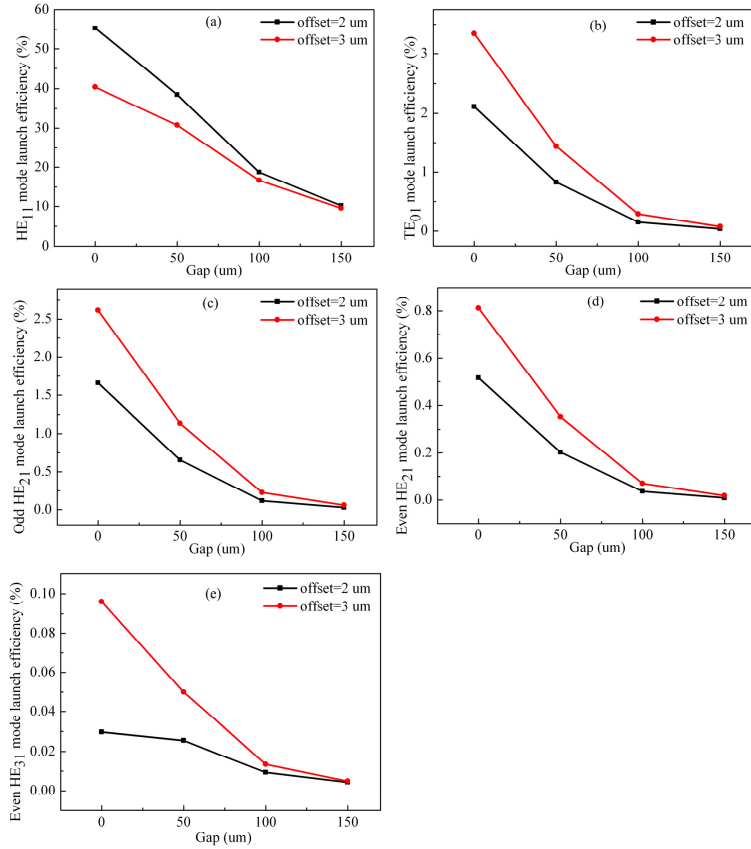


Fig. 8. Mode launch efficiency of (a) HE<sub>11</sub> mode, (b) TE<sub>01</sub> mode, (c) odd HE<sub>21</sub> mode, (d) even HE<sub>21</sub> mode, (e) even HE<sub>31</sub> mode. The black and red lines correspond to lateral offsets of 2 and 3  $\mu\text{m}$ , respectively.

#### 4. Gas detection with WMS

Wavelength modulation/harmonic detection techniques are popularly used for laser-based gas absorption measurements [22–27]. Multiple reflections occurring in gas cells were found to generate etalon fringes and produce harmonics in the output that are indistinguishable from the gas absorption signal. These etalon effects may be reduced by selecting proper modulation parameters [22, 25] and by digital signal processing [26, 27]. Here we demonstrate that similar techniques could be used to reduce the effect of MI on HC-PBF based gas sensors.

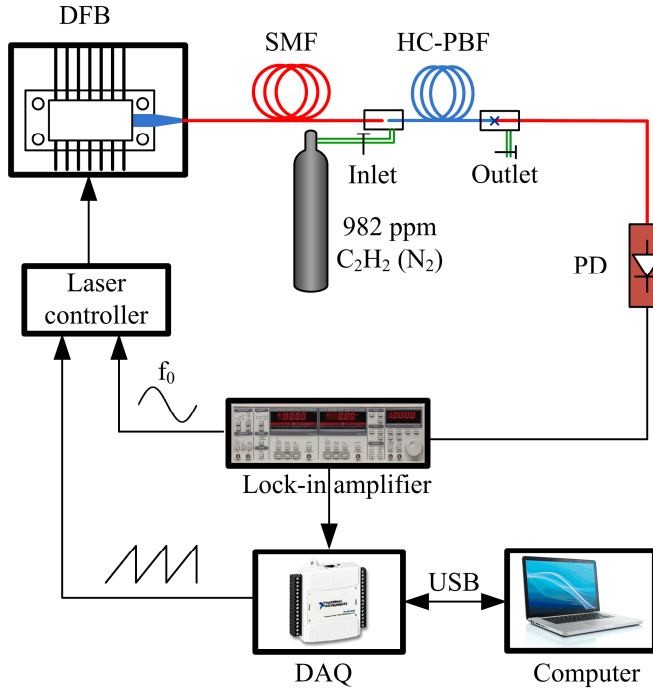


Fig. 9. Experimental setup for gas detection with WMS. DFB: distributed-feedback laser, PD: photodetector, DAQ: data acquisition.

The experimental setup with WMS is shown in Fig. 9. A  $1.53 \mu\text{m}$  distributed feedback (DFB) semiconductor laser is used as the light source and the wavelength of the laser was ramped across the P(9) absorption line of acetylene periodically and at the same time it was modulated sinusoidally at a higher frequency of  $6 \text{ kHz}$ . The second-harmonic of the modulation signal (i.e., at  $12 \text{ kHz}$ ) was detected by use of a lock-in amplifier. The output end of the HC-1550-02 fiber was spliced to SMF with low fusion current to prevent the collapse of air-holes [28]. The fusion duration and current was set to  $0.2 \text{ s}$  and  $12.5 \text{ mA}$ , and the offset and overlap were  $45$  and  $10 \mu\text{m}$ , respectively. A micro-channel was drilled from aside of the HC-PBF near the HC-PBF/SMF splicing joint by use of an  $800 \text{ nm}$  femtosecond laser. Instead of fusion splicing, the input end of a  $13 \text{ m}$  HC-1550-02 sample is mechanically spliced to SMF, with a gap between the ends of the SMF and HC-PBF. The gap serves as channel for gas filling and the size of the gap is selected for optimal mode launch described in section 3. The two connection joints were enclosed within two  $10\text{-cm-long}$  tubes with diameter of  $1 \text{ cm}$ . The input end of the tubes was connected to a high-pressure gas cylinder containing  $982 \text{ ppm}$  acetylene balanced by  $\text{N}_2$  while the other left open to atmosphere. The HC-PBF was firstly filled with the  $982 \text{ ppm}$  acetylene with  $\sim 2.5 \text{ bar}$  pressure for  $\sim 2 \text{ hours}$ , and then depressurized and sealed before taking measurements.

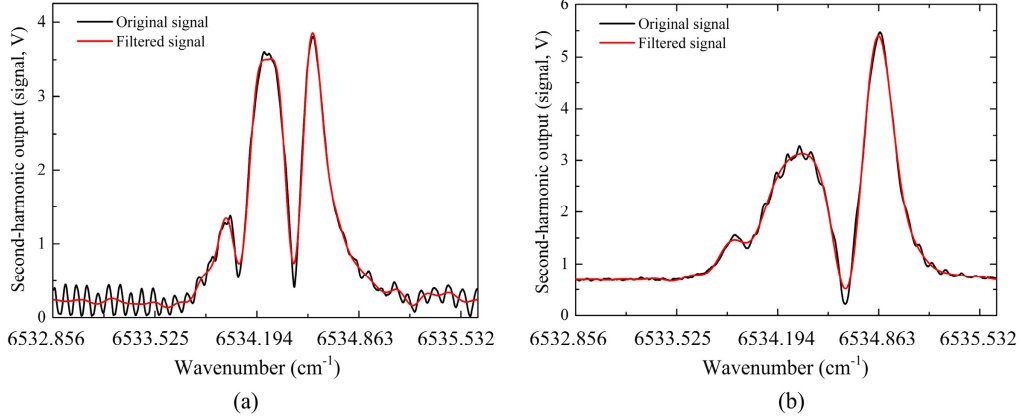


Fig. 10. Second-harmonic outputs (signals) for modulation voltages of (a) 1 V and (b) 1.9 V with wavenumber scanning across the absorption line. The black curves are the original lock-in outputs and the red curves are the results after digital filtering. (Wavenumber ( $\nu$ ) =  $1/\lambda$ )

The black lines in Fig. 10 show the second-harmonic lock-in outputs for two different modulation voltages of 1 and 1.9 volts when the laser wavenumber was scanned across the P(9) absorption line. The signal for 1.9 V (Fig. 10(b)) is bigger but fluctuates less as compared with that for 1 V (Fig. 10(a)), indicating that the signal-to-noise ratio (SNR) can be optimized by selecting proper modulation voltages. The base line in Fig. 10(b) is higher than in Fig. 10(a), and that may result from the increased residual laser intensity modulation for larger modulation voltage. At 1.9 V, the maximum second-harmonic amplitude and the base line (i.e., mean value over the wavelength region away from the absorption line) are respectively 5.5 and 0.7 V; and the standard deviation of the fluctuating signal away from the absorption is 13.7 mV, giving a SNR of 350. The lower detection limit for a SNR of unity can then be estimated to be 2.8 ppmv.

The etalon fringes have different spectral decomposition from the signal and the SNR could be further improved by digital signal processing [26, 27]. We measured the second-harmonic output signal with wavelength scanning when the HC-1550-02 fiber is free of detection gas. By analyzing the frequency contents of the second-harmonic outputs with and without detection gas, we found that they are quite different for this 13-m-long sample. The higher frequency component, which is due to MI, was further reduced by applying digital low-pass filtering after lock-in detection. Figures 10(a) and 10(b) are the original and filtered signals for two different modulation voltages. The SNRs are improved by factors of 7 and 3 for the modulation voltages of 1 and 1.9 V, respectively. The lower detection limit for an SNR of unity for 1.9 V modulation voltage is then estimated to be below 1 ppmv.

We also measured the second-harmonic output (standard deviation of the fluctuating noise when the wavelength was scanned in the wavelength range away from the absorption peak) for varying modulation voltage from 0.2 to 2.2 V. The result is shown in Fig. 11. The standard deviation for 1.9 V is minimum and about 10 times lower than for 1 V.

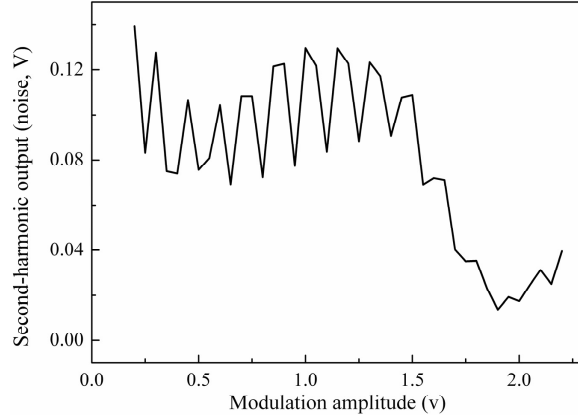


Fig. 11. Second-harmonic output (standard deviation of fluctuating noise when the wavelength was scanned in the wavelength range away from the absorption peak) as function of modulation voltage.

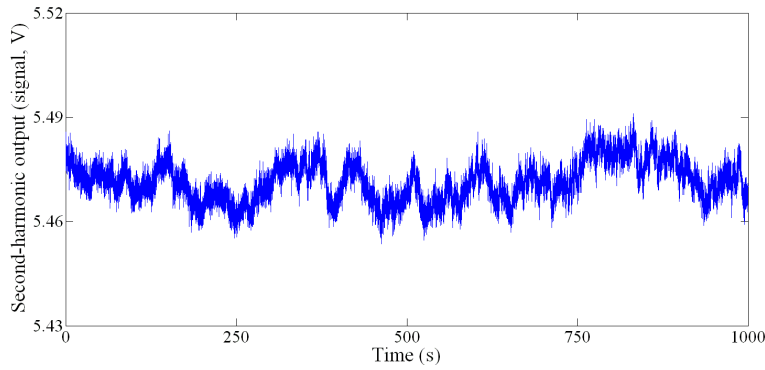


Fig. 12. Variation of second-harmonic output with time for the modulation voltage of 1.9 V. The laser wavelength was not scanned by tuned to the peak of the absorption line.

In order to investigate the signal fluctuation (noise) with a stable wavelength, we also recorded the second-harmonic output when the laser wavelength is tuned to the peak of the gas signal shown in the Fig. 10(b), and the results are shown in Fig. 12. To reduce the wavelength drift of the laser, an ultra-stable thermoelectric cooler controller was used to maintain the temperature of the DFB laser with a long-term stability of better than 0.008 °C. The time constant and slope of lock-in amplifier are set to 100 ms and 18 dB/oct, respectively. This corresponds to ~0.94 Hz detection bandwidth. The standard deviation of second-harmonic signal over a period of 1000 s is 5.5 mV, giving a SNR of 870. The low detection limit for an SNR of unity is estimated to be 1.1 ppmv.

To better understand the effect of varying modulation amplitude on the second-harmonic signal due to MI, we may analyze the second-harmonic interference signal with the theoretical model shown in Fig. 13. At the input SMF/HC-PBF splice joint, both the fundamental and higher order modes are excited, after propagating through the HC-PBF, they are combined coherently at the output splice joint and cause fluctuation in the output signal intensity. For simplicity, only one higher order mode is considered in the following.

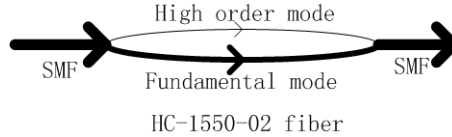


Fig. 13. Model for analyzing modal interference.

The light intensity in the output SMF may be expressed as

$$I_{\text{output}} = \langle E_{\text{output}}^2 \rangle \quad (11)$$

$$E_{\text{output}} = \sqrt{k_1 I_0} \exp(-r_1 \alpha CL) \cos(\omega(t - \tau_1)) + \sqrt{k_2 I_0} \exp(-r_2 \alpha CL) \cos(\omega(t - \tau_2)) \quad (12)$$

where  $k_1$  and  $k_2$  represent respectively the fraction light intensities,  $r_1$  and  $r_2$  the relative sensitivity factors, and  $\tau_1$  and  $\tau_2$  the group delays of the fundamental and high order modes.  $I_0$  is the input light intensity and  $\alpha$  is the (amplitude) absorption coefficient.  $r_1$  and  $r_2$  are proportional to the percentage of light power located in the air-holes [29].  $\tau_1$  and  $\tau_2$  are related to the fiber length and the group RI ( $n_{g1}$  and  $n_{g2}$ ) by:  $\tau_1 = \frac{L \cdot n_{g1}}{c}$ ,  $\tau_2 = \frac{L \cdot n_{g2}}{c}$ . For a higher order core mode,  $r_1 \approx r_2 \approx 1$ , and considering the facts that  $k_1 \gg k_2$  and in the limit of  $\alpha CL \rightarrow 0$ . Equation (11) may be approximated by

$$I_{\text{output}} \approx k_1 I_0 \left( 1 + 2\sqrt{k_1 k_2} \cos \omega \Delta \tau \right) \quad (13)$$

where  $\Delta \tau = \tau_2 - \tau_1$ . The second term in Eq. (13) is due to MI and denoted as  $I_{\text{MI}}$ .

Now, considering frequency (wavelength) modulation

$$\omega = \bar{\omega} + \delta\omega \sin(\omega_m t) \quad (14)$$

where  $\bar{\omega}$  is the frequency at the center and can be scanned by tuning the DFB laser temperature,  $\delta\omega$  the amplitude of the frequency modulation and  $\omega_m$  the modulation frequency. We have

$$\frac{I_{\text{MI}}}{k_1 I_0} = 2\sqrt{k_1 k_2} \cos \{ \bar{\omega} \Delta \tau + [\delta\omega \Delta \tau] \sin(\omega_m t) \} \quad (15)$$

Equation (15) may be expanded into its harmonic components using

$$\begin{aligned} & \cos \{ \bar{\omega} \Delta \tau + [\delta\omega \Delta \tau] \sin(\omega_m t) \} \\ &= J_0(\delta\omega \Delta \tau) \cos(\bar{\omega} \Delta \tau) - \sum_{n=1}^{\infty} A_n \sin(n\omega_m t + \theta_n) \end{aligned} \quad (16)$$

where  $A_n = 2J_n(\delta\omega \Delta \tau) \sin(\bar{\omega} \Delta \tau - \theta_n)$  and  $\theta_n = 0$  for  $n = 1, 3, 5, \dots$ ,  $\theta_n = \frac{\pi}{2}$  for  $n = 2, 4, 6, \dots$ . The amplitude of the second harmonic due to MI can then be expressed as

$$I_{\text{MI},2} \propto |J_2(\delta\omega \Delta \tau) \cos(\bar{\omega} \Delta \tau)| \quad (17)$$

From Fig. 6(b) it can be seen that the LP<sub>11</sub> mode beating with the fundamental mode dominates the MI for the 13 m long HC-1550-02 fiber sample.  $\Delta \tau$  between the LP<sub>11</sub> and fundamental modes for 13 m HC-1550-02 fiber is estimated to be  $\sim 0.433$  ns. With 1.9 V modulation amplitude, the wavelength modulation amplitude is  $\sim 118.4$  pm corresponding to  $\delta\omega \Delta \tau = 41.27$ , which determined by using an edge filter as described in [30]. The second-

harmonic noise shown in Fig. 11 as a function of  $\delta\omega\Delta\tau$  is re-drawn as the black line in Fig. 14. For comparison, the second-order Bessel function of the first kind as function of  $\delta\omega\Delta\tau$  was also calculated and shown as the red line in Fig. 14. The quasi “periodic” variation of the noise with  $\delta\omega\Delta\tau$  agrees with that of the second-order Bessel function, but the envelopes differ considerably from each other, probably due to the linear and non-linear residual amplitude modulation [31, 32]. Further work is needed to fully understand the discrepancy.

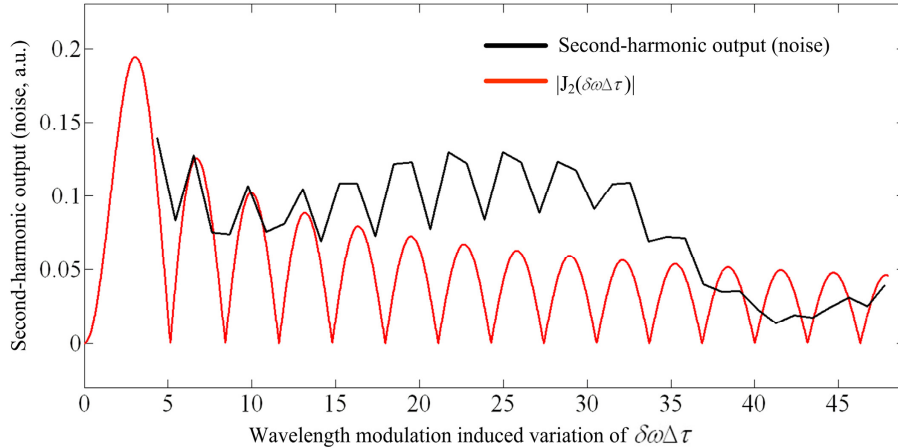


Fig. 14. Black line: the second-harmonic output (noise) calculated from the standard deviation of the fluctuating noise when the wavelength was scanned in the wavelength range away from the absorption peak, and red line: the second-order Bessel function of the first kind as function of  $\delta\omega\Delta\tau$ . The two curves are not in the same vertical scale.

## 5. Conclusion

We studied the effect of MI on the performance of HC-PBF gas sensors. The MI due to higher order core modes and cladding modes can be reduced by using a longer length of HC-PBF and the MI due to cladding modes was not observed for HC-PBF samples longer than 5 m. The MI can also be reduced by optimizing mode launch and a mechanical splice with splice gap of 100  $\mu\text{m}$  reduces the MI considerably but with an acceptable insertion for the fundamental mode. The effects of MI on the lower detection limit can be further reduced by using WMS with appropriate modulation parameters and digital signal processing. With a 13-m long HC-1550-02 sensing fiber and a combination of techniques mentioned above, we achieved a lower detection limit of less than 1 ppmv acetylene.

## Acknowledgments

This work was supported by the National Nature Science Foundation of China (NSFC) through Grant No. 61290313, the Hong Kong SAR government through a GRF grant PolyU 152064/14E, and The Hong Kong Polytechnic University through a studentship.